Meccanica (2015) 50:1747–1760
DOI 10.1007/s11012-015-0127-y

Start-up and cessation Newtonian Poiseuille and Couette flows with dynamic wall slip

George Kaoullas · Georgios C. Georgiou

Received: 30 November 2013 / Accepted: 13 February 2015 / Published online: 22 February 2015

Abstract Analytical solutions are derived for the start-up and cessation Newtonian Poiseuille and Couette flows with wall slip obeying a dynamic slip model. This slip equation allows for a relaxation time in the development of wall slip by means of a time-dependent term which forces the eigenvalue parameter to appear in the boundary conditions. The resulting spatial problem corresponds to a Sturm–Liouville problem different from that obtained using the static Navier slip condition. The orthogonality condition of the associated eigenfunctions is derived and the solutions are provided for the axisymmetric and planar Poiseuille flows and for the circular Couette flow. The effect of dynamic slip on the flow development is then discussed.

Keywords Newtonian fluid · Poiseuille flow · Start-up flow · Navier slip · Dynamic slip · Couette flow

G. Kaoullas (✉)
Oceanography Centre, University of Cyprus,
PO Box 20537, 1678 Nicosia, Cyprus
e-mail: g.kaoullas@gmail.com

G. C. Georgiou
Department of Mathematics and Statistics, University of Cyprus, PO Box 20537, 1678 Nicosia, Cyprus
e-mail: georgios@ucy.ac.cy

1 Introduction

Slip at the wall is a phenomenon observed not only with non-Newtonian [1] but also with Newtonian fluids [2]. Several slip laws have been used in the literature, the simplest one being the Navier slip law which states that the velocity of the fluid relative to that to the wall, u_w, is linearly proportional to the wall shear stress, τ_w:

$$u_w = \frac{\tau_w}{\beta} \tag{1}$$

where β is the slip coefficient, also defined as $\beta \equiv \eta/b$, where η is the viscosity and b is the slip length, i.e. the distance beyond the wall at which the fluid velocity extrapolates to zero. It should be noted that $\beta \to \infty$ is equivalent to no-slip, while $\beta = 0$ corresponds to the full-slip case.

The above slip equation, as well as, its non-linear and other extensions [1], is static, i.e. it implies that the slip velocity adjusts instantaneously to the wall shear stress. This assumption obviously holds for steady-state flows. In transient flows, however, slip relaxation effects can become important, see e.g. the slip of polymer melts [3–5]. A memory, i.e. dynamic, slip model in which the slip velocity depends on the past states of the wall shear stress has been proposed by Pearson and Petrie [6]. Its simplest version is the following extension of (1):

$$u_w + \Lambda \frac{\partial u_w}{\partial t} = \frac{\tau_w}{\beta}, \tag{2}$$

where Λ is the slip relaxation time. This model induces a delay on the development of the slip velocity. When $\Lambda = 0$, the static Navier slip model is recovered. As noted by Renardy [7] a relationship of the form (2) may arise from a competition between high stresses, which cause loss of adhesion, and a relaxation mechanism by which adhesion is restored. The experiments of Lim and Schowalter [8] on narrow molecular weight distribution polybutadienes suggested that the transition from slip to stick conditions exhibits the characteristics of a relaxation process. In an attempt to find an explanation for the melt fracture extrusion instability, Renardy [7] showed that the equations governing the two-dimensional inertialess flow of an upper-convected Maxwell fluid can become ill-posed when combined with the slip Eq. (2), leading to short-wave instabilities. However, as pointed out by Graham [9], the addition of any finite solvent viscosity to the model renders it well-posed. Black and Graham [10] suggested that this pathology may stem from the unphysical property that even if the shear stress vanishes, the model allows a finite slip velocity to persist. They thus proposed a modified dynamic slip model involving an evolution equation for the fraction of available polymer segments that are strongly interacting with the solid surface.

Other dynamic slip models have been used in the literature, such as the power-law model by Hatzikiriakos and Dealy [4], to explain the observed slip in transient shear experiments of molten polymers (high density polyethylenes). Transient observations were made for both exponential and oscillatory shear and the results were fitted with a dynamic slip model in conjunction with a Maxwell model of viscoelasticity. Hatzikiriakos and Dealy [4] pointed out that melt slip is a physicochemical process in which the polymer/wall interface may undergo continuous change with time before attaining steady state. Hatzikiriakos and Kalogerakis [5] extended the above model simulating the behaviour of a polymer/metal interface by means of a network kinetic theory. The calculated time-dependent slip velocities with experimental data on high-density polyethylene. Consequently, Hatzikiriakos [3] extended this single-mode model to a multi-mode one. Aral and Kalyon [11] investigated the time and temperature-dependent development of wall slip in the case of concentrated suspensions with Newtonian binders in steady torsional flow. They showed that for these generalised Newtonian materials there is a critical time for both the wall velocity and the shear stress to reach steady values and that this critical time decreases with increasing apparent shear rate.

Graham [9] used a power-law dynamic slip model with non-zero slip yield stress, as well as, its two-mode generalisation and noted that, both viscoelasticity and a dynamic slip model are necessary in order to explain the instabilities and nonlinear dynamics of polymer melts in oscillatory shear. Further, it was shown rigorously that for linear and weakly nonlinear viscoelasticity, in oscillatory shear with a static power-law slip law there are no non-periodic responses. Lan et al. [12] combined the dynamic slip models of [4] and [10] with different constitutive equations, such as Wagner's equation and the Liu model, to determine the slip parameters for a linear low-density polyethylene. All models gave good predictions of sliding plate rheometer slip data in steady shear by showed insufficient gap dependence in exponential shear. A multi-mode extension of slip Eq. (2), similar to the generalised Maxwell mechanical model for viscoelasticity, has been employed by Kazatchkov and Hatzikiriakos [13], giving a better fit to experimental data for molten polymers in shear flow. This new dynamic slip model involving multiple slip relaxation times was used along with Wagner's constitutive equation in solving the transient shear response of a linear low-density polyethylene, yielding improved predictions of the stress response in start-up of steady shear and large-amplitude oscillatory tests. As noted by Hatzikiriakos [1] the effect of dynamic slip has also been taken into account in stochastic simulations of polymer melts (see e.g. [3, 5, 14–16]).

In a recent paper Thalakkottor and Mohseni [17] carried out molecular dynamic simulations to study slip at the fluid-solid boundary in unsteady flow. Interestingly, their numerical experiments revealed that the slip velocity is dependent not only on the shear rate but also on fluid acceleration and follows an equation which is identical to Eq. (2). Although the original derivation was based on some characteristics of gases, it has been verified that an analogous formulation is valid for simple liquid flows.

Several analytical solutions have been reported for steady-state Newtonian, Poiseuille flows with static slip in various geometries using static slip equations, such as the Navier slip equation [18–20], and the slip

yield stress model [21, 22]. Using various static slip laws, both linear and non-linear, Ferrás et al. [23] presented solutions of Newtonian and Non-Newtonian Couette and Poiseuille flows. Additionally, analytical solutions for time-dependent, Newtonian flows with the Navier slip model (1), have also been reported in the literature [24–28]. Solutions of various start-up and cessation Newtonian flows with slip yield stress models have been reported in [29, 30]. An analytical solution corresponding to a pressure gradient varying linearly with time was also recently reported by Tang [31].

It is the purpose of this work to derive analytical solutions of the Newtonian Poiseuille flow for the planar and axisymmetric geometries and the Newtonian circular Couette flow using the dynamic slip Eq. (2). As demonstrated below, the time-dependence in the boundary condition leads to a more difficult mathematical problem to solve than its static counterpart. The spatial problem is of Sturm–Liouville type where the eigenvalue parameter appears in the boundary condition and thus, the orthogonality condition of the corresponding spatial eigenfunctions must be considered more carefully. The Sturm–Liouville problem encountered here, is a special case of more general ones which were tackled rigorously, see e.g. Churchill [32], Walter [33] and Fulton [34]. This type of problems, involving time derivatives in their boundary conditions are also common in free and forced vibration problems governed by the wave equation [35] and in problems in diffusion or in heat transfer between a solid and a fluid using the heat equation [36]. More references on these problems, as well as, on electric circuits involving long cables and diffusion processes in probability theory are provided in Fulton [34].

Despite the fact that wall slip of Newtonian fluids is supported by experimental observations [2], it can be argued that there is no justification for using a dynamic slip equation in transient Newtonian flows. The recent numerical dynamics experiments of [17] demonstrated that the dynamic slip equation applies in unsteady flows of simple liquids. Moreover, the analytical solutions derived below may be useful in checking numerical non-Newtonian simulation codes and in start up and cessation of steady shear in MEMS devices.

In Sect. 2, we consider the axisymmetric Poiseuille flow of a Newtonian fluid with dynamic wall slip. Following the solution procedure in [35], the appropriate orthogonality condition for the spatial eigenfunctions is derived, and the full procedure for the solution is given. The implications of the dynamic slip term in the slip equation are then discussed. In Sect. 3, the results for the planar Poiseuille flow are summarised. The circular Couette flow is solved analytically in Sect. 4 and finally, in Sect. 5 the conclusions of this work are provided.

2 Axisymmetric Poiseuille flow

We consider the start-up, pressure-driven flow of a Newtonian fluid in an infinitely long circular tube of radius R. The flow is assumed to be laminar, incompressible and unidirectional and gravity is neglected. In cylindrical polar coordinates, the velocity component in the z-direction, $u_z(r,t)$, satisfies

$$\rho\frac{\partial u_z}{\partial t} = G + \eta\left(\frac{\partial^2 u_z}{\partial r^2} + \frac{1}{r}\frac{\partial u_z}{\partial r}\right), \tag{3}$$

where ρ is the density and G is the constant pressure gradient. Initially the flow is at rest,

$$u_z(r,0) = 0. \tag{4}$$

As for the boundary conditions, u_z is finite along the axis of symmetry and slip is assumed along the wall following the slip law (2). Given that $\tau_w = |\tau_{rz}|_{r=R}$, one gets

$$u_w = -\frac{\eta}{\beta}\frac{\partial u_w}{\partial r} - \Lambda\frac{\partial u_w}{\partial t}. \tag{5}$$

It is clear that the steady-state solution of the problem (3)–(5), is given by

$$u^s(r) = \frac{R^2 G}{4\eta}\left[1 + 2B - \left(\frac{r}{R}\right)^2\right], \tag{6}$$

where

$$B \equiv \frac{\eta}{\beta R}, \tag{7}$$

is a dimensionless inverse slip number (where $B = 0$ corresponds to no-slip and $B \to \infty$ to the full-slip case). In order to homogenise Eq. (3) we look for solutions of the form

$$u_z(r,t) = u^s - \bar{u}_z(r,t), \tag{8}$$

where $\bar{u}$ is the solution of the homogeneous problem. Using separation of variables,

$$\bar{u}_z(r,t) = \sum_{n=1}^{\infty} X_n(r)T_n(t) \tag{9}$$

we obtain the following ordinary differential equations

$$T_n'(t) + \frac{\lambda_n^2 \nu}{R^2} T_n(t) = 0, \tag{10}$$

and

$$[rX_n'(r)]' + r\lambda_n^2/R^2 X_n(r) = 0, \tag{11}$$

where, $\nu \equiv \eta/\rho$ is the kinematic viscosity and λ_n, $n = 1, 2, \ldots$, are the eigenvalues of the problem to be determined. The boundary conditions dictate that $X_n(0)$ is finite and

$$X_n(R) = -BRX_n'(R) + \lambda_n^2 \frac{\Lambda \nu}{R^2} X_n(R). \tag{12}$$

It is worth noting that the solution to the homogeneous problem, $\bar{u}_z$, corresponds to the solution of the cessation problem. Equation (11) is Bessel's equation of zero order, which is a special type of Sturm–Liouville problem where the eigenvalues appear in the boundary condition (12). The solution to the homogeneous problem thus becomes

$$\bar{u}_z(r,t) = \sum_{n=1}^{\infty} X_n(r) e^{-\frac{\lambda_n^2 \nu}{R^2} t}, \tag{13}$$

and

$$X_n(r) \equiv A_n J_0(\lambda_n r/R) + C_n Y_0(\lambda_n r/R). \tag{14}$$

Here, J_i and Y_i are the order i Bessel functions of the first and second kind, respectively. Given that $X_n(0)$ is finite, $C_n = 0$ and Eq. (12) leads to the following transcendental equation:

$$J_0(\lambda_n) = \frac{\lambda_n B J_1(\lambda_n)}{1 - \lambda_n^2 \Lambda \nu / R^2}. \tag{15}$$

We still need to determine the coefficients A_n from the initial condition (4), which requires that

$$\sum_{n=1}^{\infty} A_n J_0(\lambda_n r/R) = u^s(r) = \frac{R^2 G}{4\eta}\left[1 + 2B - \left(\frac{r}{R}\right)^2\right]. \tag{16}$$

In such problems, one multiplies both sides of the equation above with the eigenfunction, integrates, and obtains an expression for the coefficients A_n by means of the orthogonality property of the eigenfunctions. However, since the eigenvalue appears in the boundary condition (12), the orthogonality condition must be considered more carefully.

Now we consider the one-dimensional problem in r and introduce,

$$[rX_m'(r)]' + r\lambda_m^2/R^2 X_m(r) = 0, \tag{17}$$

$$X_m(R) = -BRX_m'(R) + \lambda_m^2 \frac{\Lambda \nu}{R^2} X_m(R), \tag{18}$$

such that, X_m, X_n and λ_m, λ_n are distinct ($m \neq n$). Multiplying (11) by X_m and integrating by parts gives

$$\begin{aligned} &RX_n'(R)X_m(R) - \int_0^R rX_n'X_m' \,\mathrm{d}r \\ &\quad + \lambda_n^2 R^2 \int_0^R rX_nX_m \,\mathrm{d}r = 0. \end{aligned} \tag{19}$$

Multiplying (17) by X_n, integrating by parts, and subtracting from (19), we have

$$\begin{aligned} &R[X_n'(R)X_m(R) - X_n(R)X_m'(R)] + (\lambda_n^2 - \lambda_m^2)/R^2 \\ &\quad \int_0^R rX_nX_m \,\mathrm{d}r = 0. \end{aligned} \tag{20}$$

Using now the b.c.s. (12) and (18) we get

$$(\lambda_n^2 - \lambda_m^2)\left[\frac{\Lambda \nu}{B} X_n(R)X_m(R) + \int_0^R rX_nX_m \,\mathrm{d}r\right] = 0. \tag{21}$$

Since λ_m and λ_n are distinct

$$\frac{\Lambda \nu}{B} X_n(R)X_m(R) + \int_0^R rX_nX_m \,\mathrm{d}r = \delta_{m,n} N_n \tag{22}$$

where

$$N_n = \frac{\Lambda \nu}{B} X_n^2(R) + \int_0^R rX_n^2 \,\mathrm{d}r, \tag{23}$$

and $\delta_{m,n}$ is the Kronecker delta.

Expression (22) is the appropriate orthogonality condition for this problem, and the RHS of Eq. (23) is the square of the norm of the eigenfunctions $X_n(r)$. This result is a special case, of more general expressions on Sturm–Liouville operators, obtained by

Churchill [32], and Langer [36], and similar results also hold if the governing equation is the heat equation, i.e. in diffusion problems [36] and for the wave equation, i.e. in forced vibration problems [35]. Setting $\Lambda = 0$, the orthogonality condition (22) leads to its static counterpart [24–28].

In order to determine the coefficients A_n, Eq. (16) must be supplemented by an extra term. Thus, multiplying (16) by $rJ_0(\lambda_m r/R)$, and integrating gives

$$\int_0^R ru^s(r)J_0(\lambda_m r/R)\,\mathrm{d}r = \sum_{n=1}^{\infty} A_n \int_0^R rJ_0(\lambda_n r/R)J_0(\lambda_m r/R)\,\mathrm{d}r. \tag{24}$$

Also, consider (16) times $(\Lambda v/B)J_0(\lambda_m r/R)$ which gives

$$\frac{\Lambda v}{B}u^s(r)J_0(\lambda_m r/R) = \frac{\Lambda v}{B}\sum_{n=1}^{\infty} A_n J_0(\lambda_n r/R)J_0(\lambda_m r/R), \tag{25}$$

and when $r = R$,

$$\frac{\Lambda v}{B}u^s(R)J_0(\lambda_m) = \frac{\Lambda v}{B}\sum_{n=1}^{\infty} A_n J_0(\lambda_n)J_0(\lambda_m). \tag{26}$$

Adding (24) and (26) gives

$$\begin{aligned}&\frac{\Lambda v}{B}u^s(R)J_0(\lambda_m) + \int_0^R ru^s(r)J_0(\lambda_m)\,\mathrm{d}r \\ &\quad= \sum_{n=1}^{\infty} A_n\left[\frac{\Lambda v}{B}J_0(\lambda_n)J_0(\lambda_m) + \int_0^R rJ_0(\lambda_n r/R)J_0(\lambda_m r/R)\,\mathrm{d}r\right] \\ &\quad= \sum_{n=1}^{\infty} A_n N_n \delta_{n,m} = A_m N_m.\end{aligned} \tag{27}$$

where, the orthogonality condition (22) has been used to obtain the right-hand side of (27). Thus, the coefficients are given by

$$A_n = \frac{2R^2G}{\eta}\frac{J_1(\lambda_n)}{\lambda_n^3\left[\left(1+\frac{2\Lambda v}{BR^2}\right)J_0^2(\lambda_n)+J_1^2(\lambda_n)\right]}, \tag{28}$$

and the solution to the problem becomes

$$u_z(r,t) = \frac{R^2G}{4\eta}\left[1+2B-\left(\frac{r}{R}\right)^2 - 8\sum_{n=1}^{\infty}\frac{J_1(\lambda_n)J_0(\lambda_n r/R)e^{-\frac{\lambda_n^2 v}{R^2}t}}{\lambda_n^3\left[\left(1+\frac{2\Lambda v}{BR^2}\right)J_0^2(\lambda_n)+J_1^2(\lambda_n)\right]}\right]. \tag{29}$$

Therefore, the slip velocity is

$$u_w(t) = \frac{R^2G}{2\eta}\left[B - 4\sum_{n=1}^{\infty}\frac{J_0(\lambda_n)J_1(\lambda_n)}{\lambda_n^3\left[\left(1+\frac{2\Lambda v}{BR^2}\right)J_0^2(\lambda_n)+J_1^2(\lambda_n)\right]}e^{-\frac{\lambda_n^2 v}{R^2}t}\right] \tag{30}$$

and the volumetric flow rate is given by

$$Q(t) = \frac{\pi R^4 G}{8\eta}\left[1+4B-32\sum_{n=1}^{\infty}\frac{J_1^2(\lambda_n)}{\lambda_n^4\left[\left(1+\frac{2\Lambda v}{BR^2}\right)J_0^2(\lambda_n)+J_1^2(\lambda_n)\right]}e^{-\frac{\lambda_n^2 v}{R^2}t}\right]. \tag{31}$$

Setting $\Lambda = 0$ in Eq. (29) we obtain the solution for the static slip case

$$u_z(r,t) = \frac{R^2 G}{4\eta}\left[1 + 2B - \left(\frac{r}{R}\right)^2 - 8\sum_{n=1}^{\infty} \frac{J_0(\lambda_n r/R) e^{-\frac{\lambda_n^2 v}{R^2} t}}{\lambda_n^3 (1 + B^2\lambda_n^2) J_1(\lambda_n)}\right], \tag{32}$$

where

$$\Lambda^* = \frac{\Lambda v}{R^2}, \tag{36}$$

is the dimensionless dynamic slip number. The non-dimensional slip velocity at the wall is given by

$$u_w^*(t^*) = \frac{4}{1+4B}\left[B - 4\sum_{n=1}^{\infty} \frac{J_0(\lambda_n) J_1(\lambda_n)}{\lambda_n^3\left[\left(1 + \frac{2\Lambda^*}{B}\right) J_0^2(\lambda_n) + J_1^2(\lambda_n)\right]} e^{-\lambda_n^2 t^*}\right], \tag{37}$$

where λ_n are the roots of

$$J_0(\lambda_n) = B\lambda_n J_1(\lambda_n). \tag{33}$$

In the case of no-slip, $B = \Lambda = 0$. It turns out that λ_n are the roots of J_0 and the standard-textbook solution is obtained.

$$u_z(r,t) = \frac{R^2 G}{4\eta}\left[1 - \left(\frac{r}{R}\right)^2 - 8\sum_{n=1}^{\infty} \frac{J_0(\lambda_n r/R) e^{-\frac{\lambda_n^2 v}{R^2} t}}{\lambda_n^3 J_1(\lambda_n)}\right]. \tag{34}$$

To non-dimensionalise the solution, we scale the velocity by the mean steady-state velocity U, lengths by R, pressure by $\eta U/R$, and time by v/R^2 and denote all dimensionless variables by stars. Hence, the dimensionless velocity is given by

$$u_z^*(r^*, t^*) = \frac{2}{1+4B}\left[1 + 2B - r^{*2} - 8\sum_{n=1}^{\infty} \frac{J_1(\lambda_n) J_0(\lambda_n) e^{-\lambda_n^2 t^*}}{\lambda_n^3\left[\left(1 + \frac{2\Lambda^*}{B}\right) J_0^2(\lambda_n) + J_1^2(\lambda_n)\right]}\right], \tag{35}$$

and the dimensionless volumetric flow rate becomes

$$Q^*(t^*) = 1 - \frac{32}{1+4B}\sum_{n=1}^{\infty} \frac{J_1^2(\lambda_n)}{\lambda_n^4\left[\left(1 + \frac{2\Lambda^*}{B}\right) J_0^2(\lambda_n) + J_1^2(\lambda_n)\right]} e^{-\lambda_n^2 t^*}. \tag{38}$$

The evolution of the velocity profile for two slip numbers, $B = 0.1$ and 1 (corresponding to moderate and strong slip), and three relaxation times ($\Lambda^* = 0$, 1 and 10) is illustrated in Figs. 1 and 2. Compared to the static slip model ($\Lambda^* = 0$), it takes longer for the flow to develop to steady-state for higher values of the relaxation time. This is due to the fact that the slip boundary condition changes dynamically and the past states of the wall shear stress affect the slip velocity. This is more clearly seen in Fig. 3, which shows the evolution of the slip velocity for different values of Λ^*.

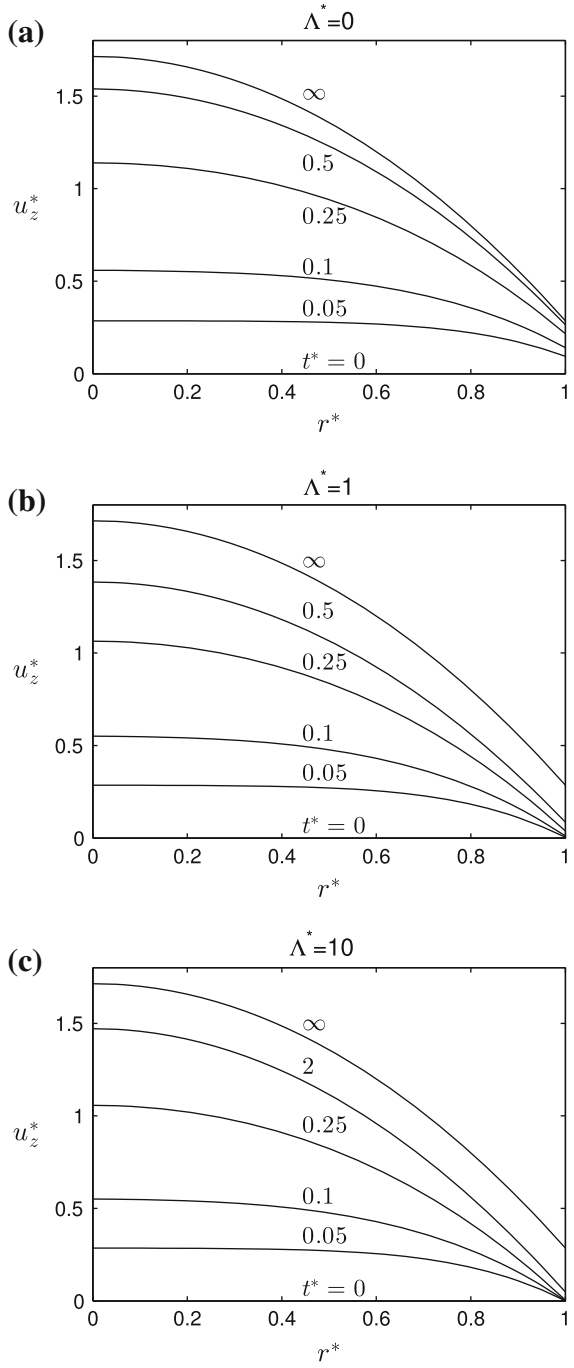

Fig. 1 Evolution of the velocity profile in start-up axisymmetric Poiseuille flow with $B = 0.1$: **a** $\Lambda^* = 0$ (static slip); **b** $\Lambda^* = 1$; and **c** $\Lambda^* = 10$

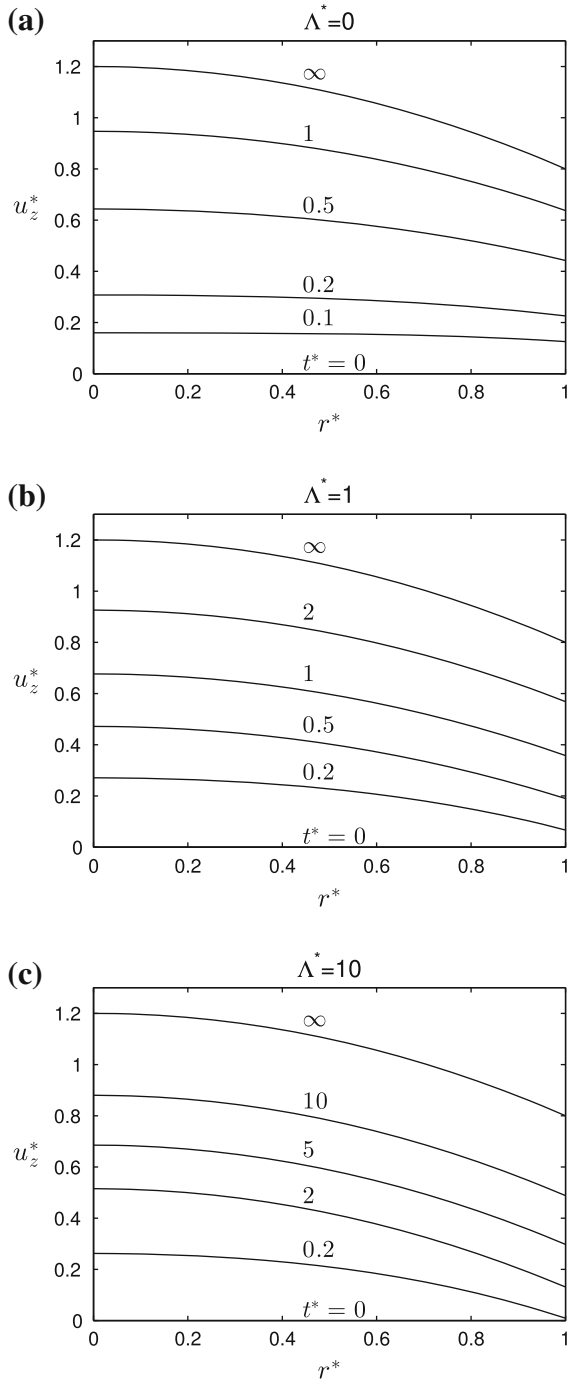

Fig. 2 Evolution of the velocity profile in start-up axisymmetric Poiseuille flow with $B = 1$: **a** $\Lambda^* = 0$ (static slip); **b** $\Lambda^* = 1$; and **c** $\Lambda^* = 10$

Similar conclusions can be drawn for the effect of the relaxation time on the evolution of the dimensionless volumetric flow rate, illustrated in Fig. 4. An interesting observation is that for higher values of B (i.e. for stronger slip), Q^* needs more time to develop, and thus at any given time, Q^* decreases with

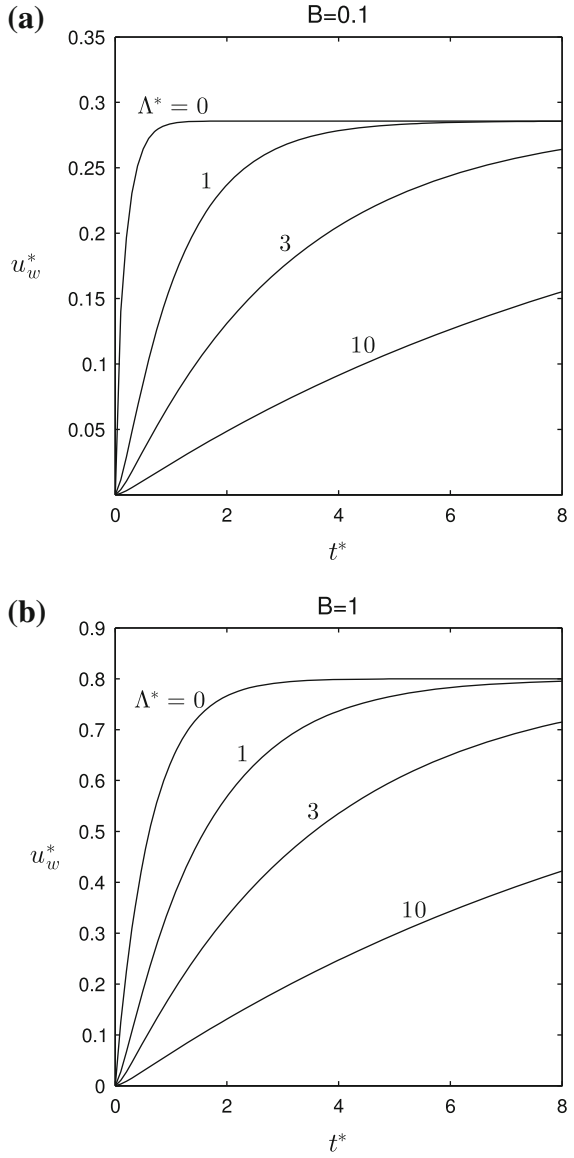

Fig. 3 Evolution of the slip velocity, in start-up axisymmetric Poiseuille flow for different values Λ^*: **a** $B = 0.1$; and **b** $B = 1$

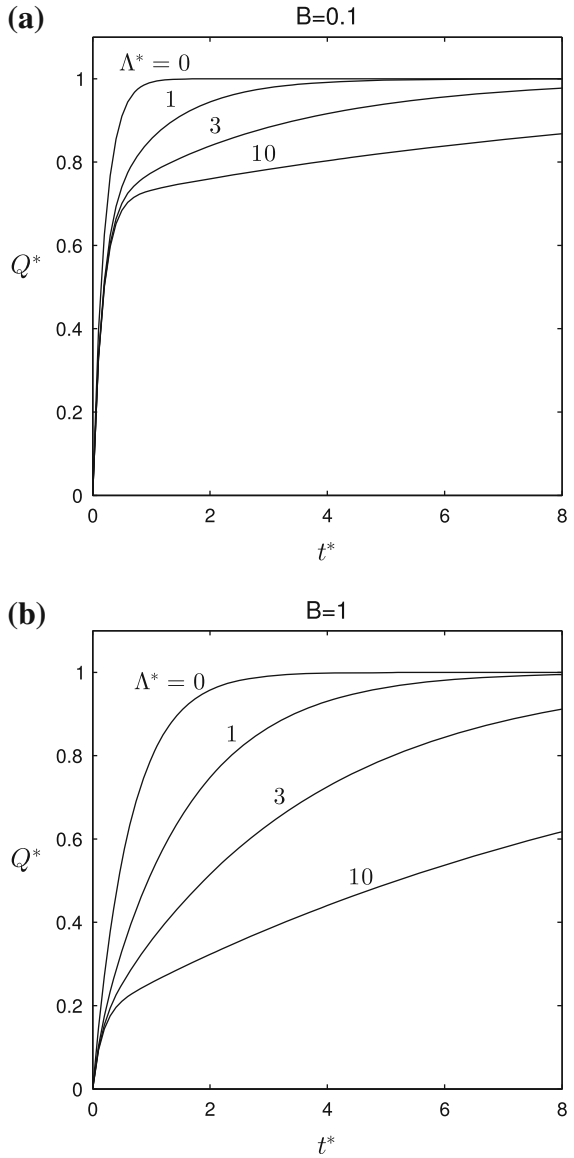

Fig. 4 Evolution of the volumetric flow rate, in start-up axisymmetric Poiseuille flow for different values of Λ^*: **a** $B = 0.1$; **b** $B = 1$

increasing B. Actually, there is more flow as B increases, which cannot be seen due to our non-dimensionalisation.

In the case of cessation i.e. when the flow is initially fully-developed flow and the pressure-gradient is suddenly set to zero, the velocity is given by:

$$u_z^*(r^*, t^*) = \frac{16}{1+4B} \sum_{n=1}^{\infty} \frac{J_1(\lambda_n) J_0(\lambda_n) e^{-\lambda_n^2 t^*}}{\lambda_n^3 \left[\left(1 + \frac{2\Lambda^*}{B} \right) J_0^2(\lambda_n) + J_1^2(\lambda_n) \right]}. \tag{39}$$

Similarly, the slip velocity and the volumetric flow rate correspond to the last terms of Eqs. (37) and (38).

3 Planar geometry

3.1 Poiseuille flow

In the case of plane Poiseuille flow in a tube with $-1 \leq y^* \leq 1$, one finds that the dimensionless velocity is given by

$$u_x^*(y^*,t^*) = \frac{3}{2(1+3B)}\left[1+2B-y^{*2}-4\sum_{n=1}^{\infty}\frac{\sin\lambda_n\cos(\lambda_n y^*)e^{-\lambda_n^2 t^*}}{\lambda_n^2\left(\frac{2\lambda_n\Lambda^*}{B}\cos^2\lambda_n+\lambda_n+\sin\lambda_n\cos\lambda_n\right)}\right], \tag{40}$$

where similar scales are used for the non-dimensionalisation, $B \equiv \eta/(\beta H)$ is the slip number, and the eigenvalues, λ_n, are the solutions of the transcendental equation

$$\tan\lambda_n = \frac{1}{B\lambda_n}(1-\Lambda^*\lambda_n^2), \tag{41}$$

where $\Lambda^* = \Lambda v/H^2$. Hence, the non-dimensional slip velocity takes the form

$$u_w^*(t^*) = \frac{3}{1+3B}\left[B-2\sum_{n=1}^{\infty}\frac{\sin\lambda_n\cos\lambda_n}{\lambda_n^2\left(\frac{2\lambda_n\Lambda^*}{B}\cos^2\lambda_n+\lambda_n+\sin\lambda_n\cos\lambda_n\right)}e^{-\lambda_n^2 t^*}\right], \tag{42}$$

and the dimensionless volumetric flow rate is given by,

$$Q^*(t^*) = 1-\frac{6}{1+3B}\sum_{n=1}^{\infty}\frac{\sin^2\lambda_n}{\lambda_n^3\left(\frac{2\lambda_n\Lambda^*}{B}\cos^2\lambda_n+\lambda_n+\sin\lambda_n\cos\lambda_n\right)}e^{-\lambda_n^2 t^*}. \tag{43}$$

Obviously, the velocity in the case of cessation is given by

$$u_x^*(y^*,t^*) = \frac{6}{2(1+3B)}\sum_{n=1}^{\infty}\frac{\sin\lambda_n\cos(\lambda_n y^*)e^{-\lambda_n^2 t^*}}{\lambda_n^2\left(\frac{2\lambda_n\Lambda^*}{B}\cos^2\lambda_n+\lambda_n+\sin\lambda_n\cos\lambda_n\right)}. \tag{44}$$

3.2 Couette flow

Here we consider the planar Couette flow in a tube with $0 \le y^* \le 1$ where the wall at $y^* = 1$ moves with speed V. One finds that the non-dimensional velocity (scaled by V) is given by

$$u_x^*(y^*, t^*) = \frac{y^* + B}{1 + 2B} - \sum_{n=1}^{\infty} C_n \left[\sin(\lambda_n y^*) + \frac{\lambda_n}{BI} \cos(\lambda_n y^*) \right] e^{-\lambda_n^2 t^*}, \quad (45)$$

where

$$C_n = \frac{(B^2\lambda_n^2 + I^2)\sin\lambda_n}{\lambda_n^2 B(I^2 + 2B + B^2\lambda_n^2 + 2\Lambda^*\lambda_n^2)}, \qquad I = 1 - \lambda_n^2\Lambda^*, \quad (46)$$

and the eigenvalues, λ_n, are the solutions of the transcendental equation

$$\tan\lambda_n = \frac{2BI\lambda_n}{B\lambda_n}(B^2\lambda_n^2 - I^2). \quad (47)$$

The non-dimensional slip velocities at $y^* = 0$, and 1 are given by

$$u_{w1}^*(t^*) = \frac{B}{1 + 2B} - \sum_{n=1}^{\infty} C_n \frac{\lambda_n}{BI} e^{-\lambda_n^2 t^*}, \quad (48)$$

and

$$u_{w2}^*(t^*) = \frac{1 + B}{1 + 2B} - \sum_{n=1}^{\infty} C_n \left(\sin\lambda_n + \frac{\lambda_n}{BI}\cos\lambda_n \right) e^{-\lambda_n^2 t^*}, \quad (49)$$

respectively. The dimensionless volumetric flow rate is given by,

$$Q^*(t^*) = 1 - \frac{6}{1 + 3B} \sum_{n=1}^{\infty} \frac{\sin^2\lambda_n}{\lambda_n^3 \left(\frac{2\lambda_n\Lambda^*}{B}\cos^2\lambda_n + \lambda_n + \sin\lambda_n\cos\lambda_n \right)} e^{-\lambda_n^2 t^*}. \quad (50)$$

In the case of cessation, the velocity is given by

$$u_x^*(y^*, t^*) = \sum_{n=1}^{\infty} C_n \left[\sin(\lambda_n y^*) + \frac{\lambda_n}{BI}\cos(\lambda_n y^*) \right] e^{-\lambda_n^2 t^*}. \quad (51)$$

4 Circular Couette flow

In this section we derive the analytical solution for the start-up Newtonian circular Couette flow, i.e. the flow between two vertical coaxial cylinders of infinite length and radii κR and R, with $0 < \kappa < 1$. The outer cylinder is stationary while the inner cylinder rotates about the common axis with angular velocity Ω, in the absence of gravity. Hence, the angular velocity component $u_\theta(r, t)$ satisfies,

$$\rho \frac{\partial u_\theta}{\partial t} = \eta \frac{\partial}{\partial r}\left(\frac{1}{r}\frac{\partial}{\partial r}(r u_\theta) \right). \quad (52)$$

The fluid is initially at rest, thus

$$u_\theta(r, 0) = 0. \quad (53)$$

We assume that both walls have the same properties, so the b.c.s. are given by

$$u_\theta = \Omega\kappa R - u_{w1}, \quad \text{on } r = \kappa R \quad (54)$$

$$u_\theta = u_{w2}, \quad \text{on } r = R, \quad (55)$$

where u_{w1} and u_{w2} are the slip velocities at the inner and outer walls, respectively. The wall shear stress is defined as

$$\tau_w = |\tau_{r\theta}| = -\eta r \frac{\partial}{\partial r}\left(\frac{u_w}{r} \right). \quad (56)$$

For this type of flow, the slip velocity at the inner wall, which is rotating, is actually decreasing with time. This is a consequence of the sign convention employed in b.c.s. (54) and (55). In start-up flow, the velocity of the fluid at both walls will be increasing, which implies that u_{w1} will be decreasing and u_{w2} will be increasing with time. Thus the appropriate slip equations are

$$u_{w1} - \Lambda \frac{\partial u_{w1}}{\partial t} = \frac{\tau_{w1}}{\beta}, \quad (57)$$

$$u_{w2} + \Lambda \frac{\partial u_{w2}}{\partial t} = \frac{\tau_{w2}}{\beta}. \tag{58}$$

Hence the b.c.s. become

$$u_\theta = \Omega\kappa R + \frac{\eta}{\beta} r \frac{\partial}{\partial r}\left(\frac{u_w}{r}\right) - \Lambda \frac{\partial u_w}{\partial t}, \quad \text{on } r = \kappa R \tag{59}$$

$$u_\theta = -\frac{\eta}{\beta} r \frac{\partial}{\partial r}\left(\frac{u_w}{r}\right) - \Lambda \frac{\partial u_w}{\partial t}, \quad \text{on } r = R. \tag{60}$$

The steady-state velocity profile is given by

$$u_\theta^s = \kappa C \Omega R \left[(2B-1)\frac{r}{R} + \frac{R}{r}\right], \tag{61}$$

where $B \equiv \eta/(\beta R)$ and

$$C = \frac{\kappa^2}{\kappa - \kappa^3 + 2B(1+\kappa^3)}. \tag{62}$$

Note that the steady-state slip velocities satisfy $u_{w2}^s = \kappa^2 u_{w1}^s$ and are given by,

$$u_{w1}^s = 2CB\Omega R/\kappa \tag{63}$$

and

$$u_{w2}^s = 2\kappa CB\Omega R. \tag{64}$$

Since the b.c. (59) is non-homogeneous we follow a similar procedure as in Sect. 2 thus, the solution to the homogeneous problem, $\bar{u}_\theta$ becomes

$$\bar{u}_\theta(r,t) = \sum_{n=1}^{\infty} D_n Z_1(\lambda_n r/R) e^{-\frac{\lambda_n^2 \nu}{R^2} t}, \tag{65}$$

where,

$$Z_1(\lambda_n r/R) \equiv J_1(\lambda_n r/R) + \delta_n Y_1(\lambda_n r/R), \tag{66}$$

and λ_n, δ_n are the nth pair of the roots of

$$B\lambda_n Z_0(\kappa\lambda_n) = \left(1 + \frac{2B}{\kappa} - \lambda_n^2 \frac{\Lambda \nu}{R^2}\right) Z_1(\kappa\lambda_n), \tag{67}$$

$$B\lambda_n Z_0(\lambda_n) = \left(-1 + 2B + \lambda_n^2 \frac{\Lambda \nu}{R^2}\right) Z_1(\lambda_n). \tag{68}$$

The appropriate orthogonality condition for the eigenfunctions Z_1 can be found as

$$\begin{aligned} &\frac{\Lambda \nu}{B}\left[Z_1(\lambda_n)Z_1(\lambda_m) + \kappa Z_1(\kappa\lambda_n)Z_1(\kappa\lambda_m)\right] \\ &\quad + \int_{\kappa R}^{R} r Z_1(\lambda_n r/R) Z_1(\lambda_m r/R)\, \mathrm{d}r = \delta_{m,n} N_n \end{aligned} \tag{69}$$

where

$$N_n = \frac{\Lambda \nu}{B}\left[Z_1^2(\lambda_n) + \kappa Z_1^2(\kappa\lambda_n)\right] + \int_{\kappa R}^{R} r Z_1^2(\lambda_n r/R)\, \mathrm{d}r, \tag{70}$$

and the coefficients in (65) are given by:

$$D_n = \frac{2\Omega\kappa RC}{\lambda_n}\left[\frac{\kappa - \kappa^3 + 2B(1+\kappa^3)}{L}\right] Z_1(\kappa\lambda_n) \tag{71}$$

where

$$\begin{aligned} L = {} & \frac{2\Lambda \nu}{R^2}\kappa\lambda_n\left[Z_1^2(\lambda_n) + \kappa Z_1^2(\kappa\lambda_n)\right] + \lambda_n\left[Z_0^2(\lambda_n)\right. \\ & \left. + Z_1^2(\lambda_n) - \kappa^2\left(Z_0^2(\kappa\lambda_n) + Z_1^2(\kappa\lambda_n)\right)\right] \\ & - 2\left[Z_0(\lambda_n)Z_1(\lambda_n) - \kappa\left(Z_0(\kappa\lambda_n)Z_1(\kappa\lambda_n)\right)\right] \end{aligned} \tag{72}$$

The solution to the full problem thus becomes,

$$\begin{aligned} &u_\theta(r,t) \\ &= \Omega\kappa RC\left[(2B-1)\frac{r}{R} + \frac{R}{r} - \sum_{n=1}^{\infty} \widetilde{D}_n Z_1\left(\frac{\lambda_n r}{R}\right) e^{-\frac{\lambda_n^2 \nu}{R^2} t}\right], \end{aligned} \tag{73}$$

where

$$\widetilde{D}_n = \frac{D_n}{CR}. \tag{74}$$

Scaling the velocity by $\Omega\kappa R$ and the rest of the quantities as in Sect. 2, the non-dimensional velocity profile is given by

$$\begin{aligned} &u_\theta^*(r^*, t^*) \\ &\quad = C\left[(2B-1)r^* + \frac{1}{r^*} - \sum_{n=1}^{\infty} \widetilde{D}_n Z_1(\lambda_n r^*) e^{-\lambda_n^2 t^*}\right] \end{aligned} \tag{75}$$

and the dimensionless slip velocities by

$$u_{w1}^*(t^*) = C\left[\frac{2B}{\kappa^2} + \sum_{n=1}^{\infty} \widetilde{D}_n Z_1(\kappa\lambda_n) e^{-\lambda_n^2 t^*}\right] \tag{76}$$

and

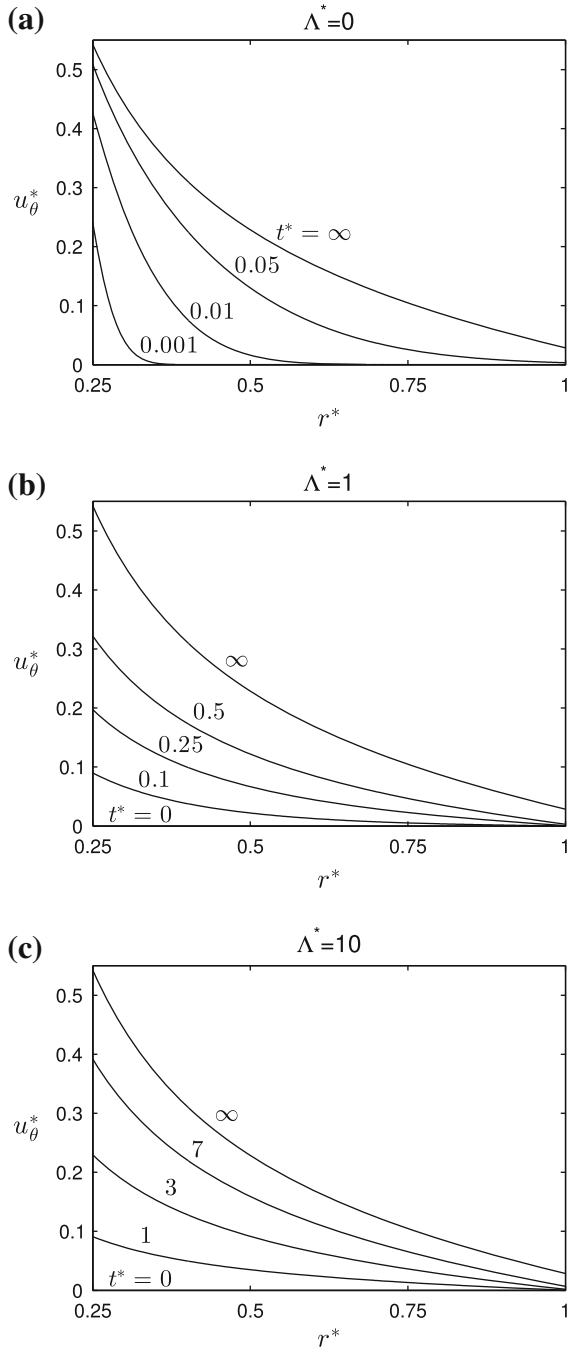

Fig. 5 Evolution of the velocity profile in start-up circular Couette flow with $B = 0.1$ and $\kappa = 0.25$: **a** $\Lambda^* = 0$; **b** $\Lambda^* = 1$; and **c** $\Lambda^* = 10$

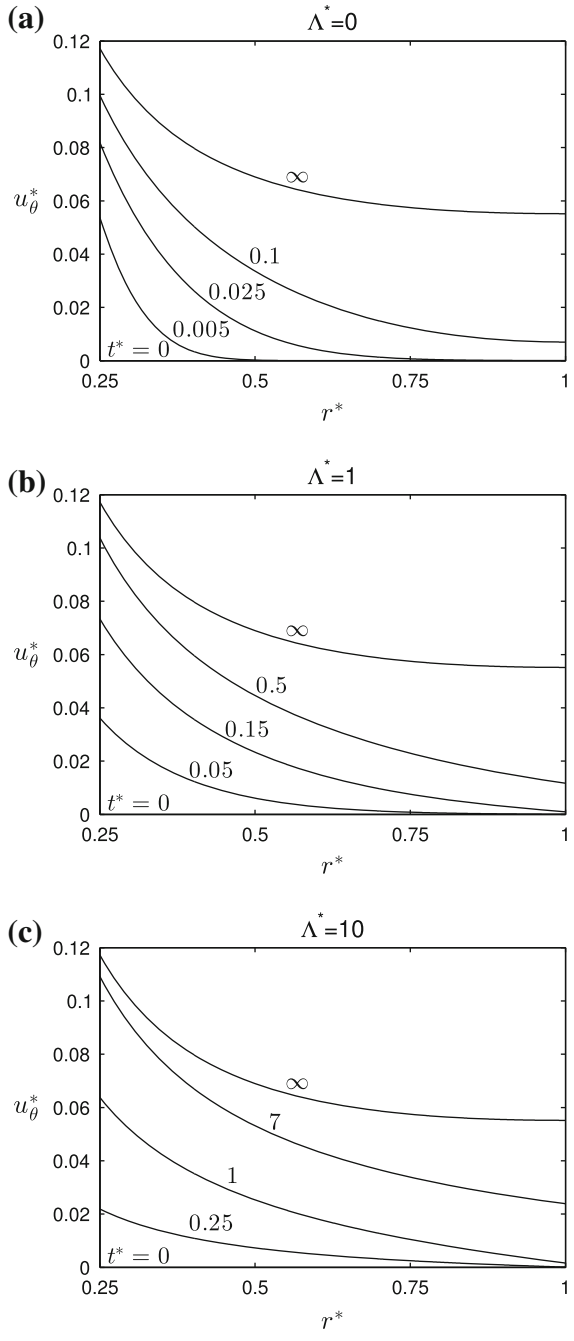

Fig. 6 Evolution of the velocity profile in start-up circular Couette flow with $B = 1$ and $\kappa = 0.25$: **a** $\Lambda^* = 0$; **b** $\Lambda^* = 1$; and **c** $\Lambda^* = 10$

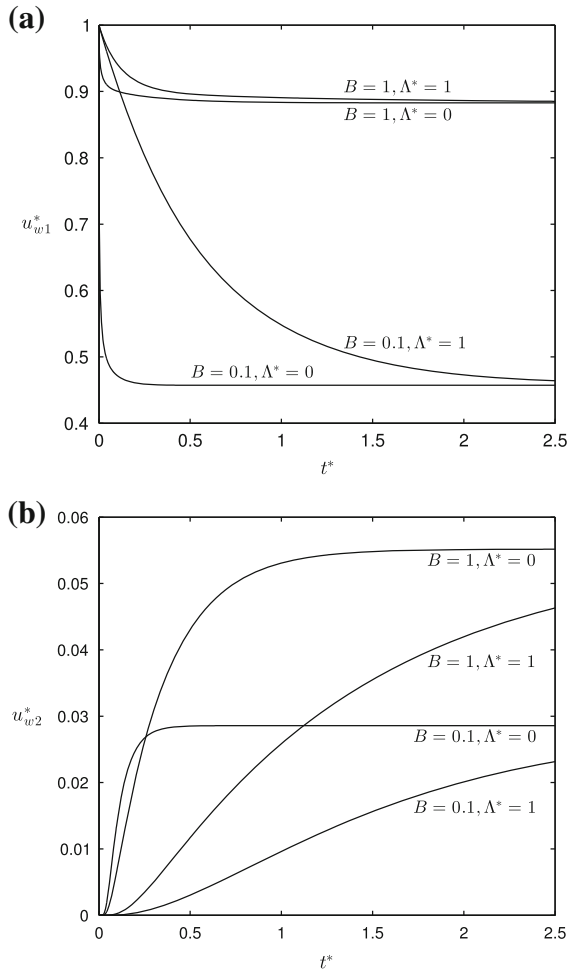

Fig. 7 Evolution of the slip velocities in start-up circular Couette flow for different values of Λ^* and $\kappa = 0.25$: **a** u^*_{w1}; and **b** u^*_{w2}

$$u^*_{w2}(t^*) = C\left[2B - \sum_{n=1}^{\infty} \widetilde{D}_n Z_1(\lambda_n) e^{-\lambda_n^2 t^*}\right]. \tag{77}$$

In the case of cessation, the velocity is given by

$$u^*_\theta(r^*, t^*) = C\left[(2B-1)r^* + \frac{1}{r^*} - \sum_{n=1}^{\infty} \widetilde{D}_n Z_1(\lambda_n r^*) e^{-\lambda_n^2 t^*}\right]. \tag{78}$$

In Figs. 5 and 6, the evolution of the velocity profile is plotted, for slip numbers, $B = 0.1$, and $B = 1$, respectively, $\kappa = 0.25$ and three relaxation times ($\Lambda^* = 0.1$, 1 and 10). Similarly to the axisymmetric Poiseuille problem, higher values of Λ^* increase the time that the velocity evolves to steady-state. In the no-slip case ($B = 0$), the fluid velocity at the inner wall, which is rotating, is always constant and equals the speed of rotation. However, it can be seen here where slip is present that the fluid velocity at the inner wall evolves gradually to its steady-state value, and it is always less than the speed of rotation. This can also be inferred indirectly from Fig. 7, which shows the evolution of the two slip velocities for two slip numbers ($B = 0.1$ and 1) and two relaxation times ($\Lambda^* = 0$ and 1). The slip velocity at the inner wall initially, equals the speed of rotation and then drops eventually to its steady-state value u^{*s}_{w1}. On the other hand, u^*_{w2} increases with time to reach the steady-state value $u^{*s}_{w2} = \kappa^2 u^{*s}_{w1}$.

5 Conclusions

We have derived analytical solutions for the start-up Newtonian Poiseuille and Couette flows with dynamic wall slip. For this purpose, the appropriate orthogonality condition for the spatial eigenfunctions has been derived. Under a dynamic slip condition, the slip velocity rather than depending on the instantaneous value of the wall shear stress, also depends on its past states. This effect delays the evolution of the slip velocity, and also the flow development.

References

1. Hatzikiriakos SG (2012) Wall slip of molten polymers. Prog Polym Sci 37(4):624–643
2. Neto C, Evans DR, Bonaccurso E, Butt HJ, Craig VSJ (2005) Boundary slip in Newtonian liquids: a review of experimental studies. Rep Progr Phys 68(12):2859–2897
3. Hatzikiriakos SG (1995) A multimode interfacial constitutive equation for molten polymers. J Rheol 39(1):61–71
4. Hatzikiriakos SG, Dealy JM (1991) Wall slip of molten high density polyethylene. i. sliding plate rheometer studies. J Rheol 35(4):497–523
5. Hatzikiriakos SG, Kalogerakis N (1994) A dynamic slip velocity model for molten polymers based on a network kinetic theory. Rheol Acta 33(1):38–47
6. Pearson JRA, Petrie CJS (1968) On melt flow instability of extruded polymers. In: Wetton RE, Whorlow RW (eds) Polymer systems: deformation and flow. McMillan, London, pp 163–187
7. Renardy M (1990) Short wave instabilities resulting from memory slip. J Non-Newton Fluid Mech 35(1):73–76

8. Lim FJ, Schowalter WR (1989) Wall slip of narrow molecular weight distribution polybutadienes. J Rheol 33(8):1359–1382
9. Graham MD (1995) Wall slip and the nonlinear dynamics of large amplitude oscillatory shear flows. J Rheol 39(4):697–712
10. Black WB, Graham MD (1996) Wall-slip and polymer-melt flow instability. Phys Rev Lett 77:956–959
11. Aral BK, Kalyon DM (1994) Effects of temperature and surface roughness on time-dependent development of wall slip in steady torsional flow of concentrated suspensions. J Rheol 38(4):957–972
12. Lan SK, Giacomin AJ, Ding F (2000) Dynamic slip and nonlinear viscoelasticity. Polym Eng Sci 40(2):507–524
13. Kazatchkov IB, Hatzikiriakos SG (2010) Relaxation effects of slip in shear flow of linear molten polymers. Rheol Acta 49(3):267–274
14. Gratton Y, Slater GW (2005) Molecular dynamics study of tethered polymers in shear flow. Eur Phys J E 17(4):455–65
15. Olgun U, Kalyon DM (2005) Use of molecular dynamics to investigate polymer meltmetal wall interactions. Polymer 46(22):9423–9433
16. Xu F, Denn MM, Schieber JD (2007) Stochastic chain simulation of wall slip in entangled polymer melts. J Rheol 51(3):451–464
17. Thalakkottor JJ, Mohseni K (2013) Analysis of boundary slip in a flow with an oscillating wall. Phys Rev E 87(033):018
18. Duan ZP, Muzychka YS (2007a) Slip flow in elliptic microchannels. Int J Therm Sci 46(11):1104–1111
19. Duan ZP, Muzychka YS (2007b) Slip flow in non-circular microchannels. Microfluid Nanofluid 3(4):473–484
20. Ebert WA, Sparrow EM (1965) Slip flow in rectangular and annular ducts. J Basic Eng 87(4):1018–1024
21. Kaoullas G, Georgiou GC (2013) Newtonian Poiseuille flows with slip and non-zero slip yield stress. J Non-Newton Fluid Mech 197:24–30
22. Spikes H, Granick S (2003) Equation for slip of simple liquids at smooth solid surfaces. Langmuir 19:5065–5071
23. Ferrás LL, Nóbrega JM, Pinho FT (2012) Analytical solutions for Newtonian and inelastic non-Newtonian flows with wall slip. J Non-Newton Fluid Mech 175–176:76–88
24. King MR (2007) Oscillatory gas flow in a circular nanotube. Open Nanosci J 1(1):1–4
25. Majdalani J (2008) Exact Navier–Stokes solution for pulsatory viscous channel flow with arbitrary pressure gradient. J Propul Power 24(6):1412–1423
26. Matthews MT, Hill JM (2008) Nanofluidics and the Navier boundary condition. Int J Nanotechnol 5(2/3):218–242
27. Wiwatanapataphee B, Wu YH, Hu M, Chayantrakom K (2009) A study of transient flows of Newtonian fluids through micro-annuals with a slip boundary. J Phys A: Math Theor 42(6):065,206
28. Wu YH, Wiwatanapataphee B, Hu M (2008) Pressure-driven transient flows of Newtonian fluids through microtubes with slip boundary. Phys A: Stat Mech Appl 387(24): 5979–5990
29. Kaoullas G, Georgiou GC (2013b) Slip yield stress effects in start-up Newtonian Poiseuille flows. Rheol Acta 52:913–925
30. Damianou Y, Philippou M, Kaoullas G, Georgiou GC (2014) Cessation of viscoplastic Poiseuille flow with wall slip. J Non-Newton Fluid Mech 203:24–37
31. Tang HS (2012) Analysis on creeping channel flows of compressible fluids subject to wall slip. Rheol Acta 51(5):421–439
32. Churchill RV (1942) Expansions in series of non-orthogonal functions. Bull Am Math Soc 48(2):143–149
33. Walter J (1973) Regular eigenvalue problems with eigenparameter in the boundary conditions. Math Z 133:301312
34. Fulton CT (1977) Two-point boundary value problems with eigenvalue parameter contained in the boundary conditions. Proc Roy Soc Edinb 77:293–308
35. Anderson GL, Thomas CR (1971) A forced vibration problem involving time derivatives in the boundary conditions. J Sound Vib 14(2):193–214
36. Langer RE (1932) A problem in diffusion or in the flow of heat for a solid in contact with a fluid. Tohoku Math J 35:260–275